Remote Sensing of Environment xxx (xxxx) 113670

Contents lists available at ScienceDirect

Remote Sensing of Environment

journal homepage: www.elsevier.com/locate/rse

First evaluation of fire severity retrieval from PRISMA hyperspectral data

Carmen Quintano [a, b], Leonor Calvo [c], Alfonso Fernández-Manso [d], Susana Suárez-Seoane [e], Paulo M. Fernandes [f], José Manuel Fernández-Guisuraga [c, f, *]

[a] Electronic Technology Department, School of Industrial Engineering, University of Valladolid, 47011 Valladolid, Spain
[b] Sustainable Forest Management Research Institute, University of Valladolid-Spanish National Institute for Agriculture and Food Research and Technology (INIA), 34004 Palencia, Spain
[c] Department of Biodiversity and Environmental Management, Faculty of Biological and Environmental Sciences, University of León, 24071 León, Spain
[d] Agrarian Science and Engineering Department, School of Agricultural and Forestry Engineering, University of León, 24400 Ponferrada, Spain
[e] Department of Organisms and Systems Biology (Ecology Unit) and Research Institute of Biodiversity (IMIB; UO-CSIC-PA), University of Oviedo, Oviedo and Mieres, Spain
[f] Centro de Investigação e de Tecnologias Agroambientais e Biológicas, Universidade de Trás-os-Montes e Alto Douro, 5000-801 Vila Real, Portugal

ARTICLE INFO

Edited by Dr. Marie Weiss

Keywords:
CBI
MESMA
PRISMA
Sentinel-2
Spaceborne spectrometers
Wildfire

ABSTRACT

The unprecedented availability of spaceborne hyperspectral data has great potential to provide fire severity estimates that align with post-fire management needs, overcoming complex logistics and data acquisition costs of airborne hyperspectral sensors, and the suboptimal sensitivity of broadband data to several post-fire ground components. We analyzed the feasibility of the PRISMA mission -one of the first spaceborne spectrometers operationally active- to assess fire severity by leveraging hyperspectral data dimensionality through the retrieval of sub-pixel components directly related to fire severity in the field. Multispectral data provided by Sentinel-2, commonly used in fire severity quantitative assessments, were used as a benchmark method. Multiple endmember spectral mixture analysis (MESMA) was used to retrieve fractional cover of char, photosynthetic vegetation (PV), as well as non-photosynthetic vegetation and soil (NPVS) from post-fire PRISMA Level 2D and Sentinel-2 Level 2A scenes in one of the largest wildfires ever recorded in the western Mediterranean Basin. Ground-truth data were obtained using the Composite Burn Index (CBI) to procure three field-measured severity metrics: vegetation, soil and site. The relationship between the CBI data on a continuum scale and the cover of char, PV and NPVS image fractions retrieved from PRISMA and Sentinel-2 was assessed through Random Forest regression (RFR). Likewise, Ordinal Forests (OF) algorithm was used to classify categorized CBI data (low, moderate and high fire severity). PRISMA-based RFR fire severity estimates at vegetation, soil and site levels (R^2 = 0.64–0.79 and RMSE = 0.33–0.41) outperformed those of Sentinel-2 (R^2 = 0.27–0.53 and RMSE = 0.54–0.60), and were in line with previous studies using airborne hyperspectral sensors at higher spatial resolution. Fire severity underestimation for high field CBI values was almost unnoticeable in the PRISMA estimates. Categorical fire severity, not currently estimated using hyperspectral data but with high interest in post-fire management, were accurately predicted by PRISMA-based OF classification, with consistent user's and producer's accuracy for each fire severity category. The high confusion between moderate and low/high fire severity categories, typical when unmixing broadband multispectral data, was overcome by the PRISMA-based classification scheme. Our results suggest that new spaceborne spectrometer missions can support reliable fire severity assessments equivalent to airborne spectrometers, but readily applicable to large-scale assessments of extreme wildfire events.

1. Introduction

Fire is a recurrent disturbance in terrestrial ecosystems of the Mediterranean basin (Pausas et al., 2008) and an evolutionary force shaping landscape patterns (Keeley et al., 2012; Arnan et al., 2013; Fernandes, 2013) and adaptive traits of species in fire-prone vegetation communities for millennia (Keeley et al., 2011; Johnstone et al., 2016). In the last decades, land use changes involving rural abandonment, together with fire suppression policies and lack of adaptive forest management, have promoted dense and continuous flammable fuels in this region (Moreira et al., 2011; Fernandes, 2013; Pausas and Keeley, 2014). In the same way, an increase in heat waves and prolonged

* Corresponding author at: Department of Biodiversity and Environmental Management, Faculty of Biological and Environmental Sciences, University of León, 24071 León, Spain.
E-mail address: joseg@utad.pt (J.M. Fernández-Guisuraga).

https://doi.org/10.1016/j.rse.2023.113670
Received 24 January 2023; Received in revised form 16 May 2023; Accepted 4 June 2023
0034-4257/

droughts, in the context of anthropogenic climate change (Giorgi and Lionello, 2008), promote fuel dryness conducive to extreme fire events (Pausas, 2004) with unprecedented ecological consequences (Fernández-Guisuraga et al., 2019; Lasslop et al., 2019). In this context, the year 2022 registered the most severe drought for 500 years in Europe, which coincided with an extreme fire season in which a burned area of about 8600 km² was reported in the European Union (European Commission, 2022). Under this scenario, extensive areas are expected to burn at high fire severity because of the connection between large wildfire spread and extreme fire behavior determined by fuel, topography and fire weather drivers (Lutz et al., 2009; Harvey et al., 2016).

Fire severity, broadly defined as the magnitude of the ecological change in a burned area with respect to the pre-fire scenario (Lentile et al., 2006), and operationally measured qualitatively as the fire effects on vegetation and soils (Key and Benson, 2005), is one of the most used fire regime attributes to measure ecological impact of wildfires (Keeley, 2009). Fire severity can be thoroughly assessed in the field using single vegetation and soil indicators (e.g. Hammill and Bradstock, 2006; Miller et al., 2009; Vega et al., 2013), or integrated indices such as the Composite Burn Index (CBI; Key and Benson, 2005). However, the exclusive use of field-based indicators is not feasible for assessing large fires because of the associated costs in time and resources (Fernández-Manso et al., 2019). For this reason, remote sensing-based assessments of fire severity are increasingly used, together with accurate field data for validation. Conventionally, spectral indices computed from broadband multispectral remote sensing data have been used to assess fire severity through empirical models (e.g. the differenced Normalized Burn Ratio -dNBR-; Key, 2006). These indices, often computed from multispectral imagery acquired by Landsat and Sentinel-2 missions, have been used extensively in many scientific studies throughout the world (e.g. Roy et al., 2006; Norton et al., 2009; Fernández-Manso et al., 2016a; Fernández-García et al., 2018a; Delcourt et al., 2021) and also operationally in the Monitoring Trends in Burn Severity (MTBS) program of the United States (Eidenshink et al., 2007; Picotte et al., 2020). However, previous research identified several drawbacks in this approach, namely: (i) its site or ecosystem-specific nature (Lentile et al., 2009) that hinders potential model transferability (Epting et al., 2005); (ii) the suboptimal performance of the limited spectral bands considered (Lentile et al., 2009); (iii) the inability to discriminate intermediate fire severity levels (Tanase et al., 2011); and (iv) the lower sensitivity to the spatial variation in fire effects at high severities than other methods such as spectral unmixing (Kolden et al., 2015).

Physically-based methods, conventionally applied to broadband multispectral data, such as spectral mixture analysis (SMA) and radiative transfer models (RTMs), are a sounder approach to provide meaningful fire severity estimates. For this purpose, RTMs have been used to simulate the spectral response of plant communities as a result of fire-induced changes and retrieve fire severity in a continuum scale from satellite imagery (e.g. Chuvieco et al., 2007; De Santis et al., 2009, 2010; Yin et al., 2020), considering the physical link between biophysical or structural variation of the canopy and the plant community reflectance (Wang et al., 2022). RTMs parametrization that meets the assumptions of plant communities with a complex structure is challenging (Yebra et al., 2008), and requires sampling many vegetation biophysical descriptors in the field to alleviate the ill-posed nature of the models (Combal et al., 2003), but this demand is not usually operative in the short term after the fire in the context of emergency-management action needs (Fernández-Guisuraga et al., 2021a). Fraction images obtained from sub-pixel image analyses, including SMA-family techniques, are a solid alternative to retrieve fire severity from satellite imagery in heterogeneous post-fire environments (Quintano et al., 2006; Lentile et al., 2009). In this sense, the retrieval of fire severity can be considered a sub-pixel matter at moderate spatial resolutions (Quintano et al., 2013) because a complex mixture of char, vegetation and soil usually defines short-term scenes after fire (Meng et al., 2017; Fernández-Manso et al., 2019). For that reason, sub-pixel techniques have a sound physical sense in post-fire environments (Quintano et al., 2012), are more readily scalable than RTMs (Meng et al., 2017) and do not require field data for calibration purposes (Somers et al., 2012; Quintano et al., 2020). Multiple endmember SMA (MESMA; Roberts et al., 1998) has been one of the most widely considered sub-pixel image analyses for fire severity estimation in recent years, mainly by retrieving the char fraction from Landsat or Sentinel-2 data (e.g. Quintano et al., 2019; Meng et al., 2017). Compared to the conventional linear SMA (LSMA; Adams et al., 1986), MESMA accounts for land cover spectral variability by allowing multiple spectra to be incorporated for each endmember and different endmember combinations to unmix each pixel in the modeling scheme (Roberts et al., 1998).

Although MESMA enabled successfully unmixing of broadband multispectral data in previous fire severity studies, a higher sensitivity to variations of fire effects on vegetation and soils may be procured when using narrowband remote sensing data as demonstrated by van Wagtendonk et al. (2004), Kokaly et al. (2007) and Veraverbeke et al. (2014) using Airborne Visible and Infrared Imaging Spectrometer (AVIRIS) and Landsat (ETM+/OLI) data. In particular, MESMA is highly suitable for hyperspectral data unmixing because the large number of narrow and spectrally contiguous bands provides enhanced spectral information to discriminate the basic components (i.e. endmembers) of the target fraction images in complex post-fire environments (Tane et al., 2018). For example, Veraverbeke et al. (2014) used weighted MESMA to compare the performance of narrowband (AVIRIS) and broadband (Landsat OLI) data for assessing fire severity in western United States. They found that the data dimensionality of AVIRIS enhanced image fraction estimates compared to Landsat OLI, and thus the correlation with field-measured fire severity. The use of airborne hyperspectral sensors such as AVIRIS (Green et al., 1998) or HyMap (Cocks et al., 1998) in operational fire severity assessments is constrained by the low spatial coverage and logistics inherent to these platforms (Veraverbeke et al., 2014; Cotrufo et al., 2018; Singh et al., 2020) with respect to spaceborne sensors.

Alternatively, Fernández-Manso et al. (2019) mapped fire severity in eastern Spain using a MESMA char fraction computed from the Hyperion sensor (Middleton et al., 2013) onboard the Earth Observing-1 satellite (EO-1), the only full-range spaceborne spectrometer in orbit (Goetz, 2009) until it was decommissioned on March 2017. Despite the success of Hyperion in a number of research fields, the narrow swath width restricted its applicability to relatively small target areas (Middleton et al., 2013). The *PRecursore IperSpettrale della Missione Applicativa* (PRISMA) mission, launched in March 2019, is considered a follow-up of pioneering Hyperion mission and offers to advance our expertise in advanced remote sensing of large burned areas from the unprecedented availability of 400–2500 nm hyperspectral satellite data with a swath width of 30 km. Details on the PRISMA mission are provided in section 2.2. In the field of remote sensing of fire disturbances, the potentiality of PRISMA hyperspectral data has been explored to date in the mapping of forest fuels and burned area (Lazzeri et al., 2021; Shaik et al., 2022), as well as in active fire detection (Amici and Piscini, 2021), but not in studies related to fire severity. Accordingly, this study explores for the first time the potential of PRISMA hyperspectral scenes to provide meaningful, physically-based fire severity estimates through the retrieval of ground cover fractions. This is particularly relevant for one of the first hyperspectral spaceborne missions, together with the Environmental Mapping and Analysis Program (EnMAP) or the Advanced Hyperspectral Imager (AHSI) onboard GaoFen-5 (GF-5) satellite, that would make possible large-scale assessments of fire severity (Veraverbeke et al., 2018). Specifically, we used MESMA to retrieve fractional cover of typical post-fire ground components (i.e. char, photosynthetic vegetation and soil) from a post-fire PRISMA scene, and estimate field-measured fire severity using multispectral Sentinel-2 retrievals as benchmark in one of the largest wildfires ever recorded in

the western Mediterranean Basin. The prediction performance was evaluated not only in terms of continuum fire severity per strata, but also using categorized fire severity data, with special emphasis in intermediate fire severity effects. We also examined the influence of plant community type on fire severity retrieval performance.

Although previous studies have widely implemented physical-based approaches to assess fire severity using multispectral sensors, including radiative transfer models (e.g. De Santis and Chuvieco, 2007; Fernández-Guisuraga et al., 2023) and MESMA (e.g. Quintano et al., 2013; Fernández-Manso et al., 2016b), the leverage of hyperspectral data and physical-based models for this purpose is scarce and limited to airborne hyperspectral sensors (Veraverbeke et al., 2014; Tane et al., 2018) or to the technology-demonstrator Hyperion imaging spectrometer (Fernández-Manso et al., 2019). To the best of our knowledge, the potential of physically-based, fire severity estimates retrieved from recent spaceborne spectrometers has not been unraveled. This represents an important gap in the scientific knowledge since hyperspectral data acquired from recent spaceborne spectrometers feature differential characteristics to previous sensors, namely a higher signal-to-noise ratio than Hyperion data (Papeş et al., 2010; Cogliati et al., 2021), but lower spatial resolution than airborne hyperspectral data (Lewis et al., 2007). The impact of these differential characteristics must be determined when using generalizable physical-based models in the face of recent and upcoming spaceborne spectrometers which will potentially allow for operational assessments of fire severity in extreme wildfire events (Veraverbeke et al., 2018). Also, this is the first study to evaluate the potential of the high dimensionality of hyperspectral data in predicting field estimates of fire severity by community strata (i.e. individual CBI scores at the soil, vegetation and site levels), which is one of the most requested procedures by land managers to identify priority areas for post-fire management. (Fernández-Guisuraga et al., 2023).

2. Material and methods

2.1. Study site and fire severity assessment in the field

The case-study site is an extreme wildfire event that burned 28,046 ha of forest, woodland, shrubland and grassland plant communities between June 15th and 19th, 2022 in the Sierra de la Culebra (northwest Iberian Peninsula; Fig. 1). The wildfire was the second largest ever recorded in Spain. Orography is characterized by steep hillsides and wide valleys, with altitude ranging between 747 and 1205 m above the sea level. Climate is Mediterranean, with mean annual temperature and precipitation of 11 °C and 750 mm, respectively (Ninyerola et al., 2005). Extreme fire weather conditions were recorded during fire spread (Rodrigues et al., 2023) as a consequence of a heat wave that occurred between June 11th and 20th (Regional Forestry Service personal communication). Also, a severe drought was recorded in the spring season preceding the fire date. The wildfire affected *Pinus sylvestris* L. (Scots pine) and *Pinus pinaster* Ait. (maritime pine) forests, *Quercus ilex* L. (holm oak) and *Quercus pyrenaica* Willd. (Pyrenean oak) woodlands, shrublands dominated by *Cistus ladanifer* L., *Pterospartum tridentatum* (L.) Willk., *Erica australis* L., and *Halimium lasianthum* subsp. *alyssoides* (Lam.) Greuter, and Mediterranean grasslands. Fire behavior was extreme in maritime pine stands and shrublands, but moderate fire

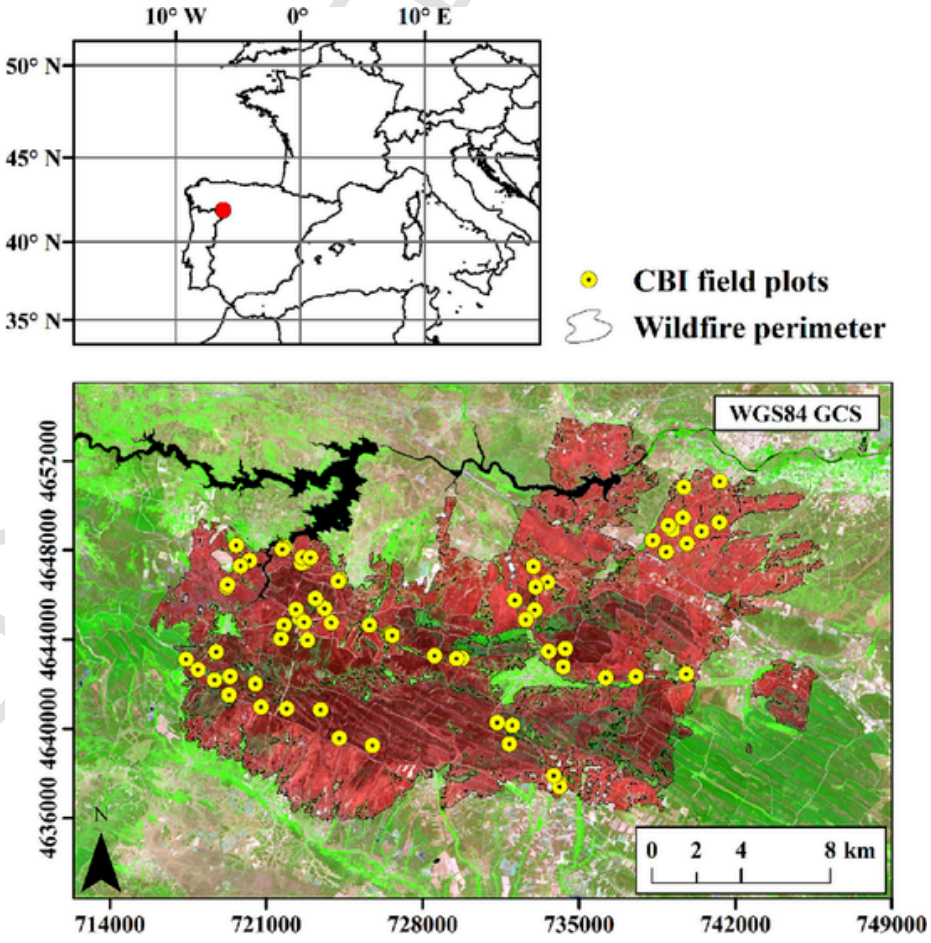

Fig. 1. Sierra de la Culebra wildfire in the western Mediterranean Basin (NW Iberian Peninsula), and distribution of the field plots where the Composite Burn Index (CBI) was assessed within the fire scar. The background image is a Sentinel-2 false color composite (R = band 12; G = band 8A; B = band 4).

effects prevailed in Scots pine and oak woodlands/forests (Regional Forestry Service, personal communication).

One month after the wildfire (July 2022), we assessed fire severity in 70 field plots of 30 m × 30 m. We used a slightly modified version (Fernández-García et al., 2018a) of the Composite Burn Index (CBI; Key and Benson, 2005) in which we did not consider attributes related to extended fire severity assessments (e.g. colonizers or change in species composition), or those related to burned legacies that were not significantly present in the study site (e.g. heavy fuel consumption in the substrate). Previous studies (Quintano et al., 2019; Fernández-Guisuraga et al., 2021a, 2023; Huerta et al., 2022) have shown the suitability of these CBI modifications in Mediterranean plant communities similar to those in our study site. Plots were georeferenced using a GPS receiver with $RMSE_{X,Y} < 1$ m and established in areas with homogeneous fire effects to ensure uniform spectral responses. Sampling design was randomly stratified, using the dominant plant communities as strata (excluding grasslands). In the understory layer, we recorded fine fuel consumption and char attributes for the substrate stratum. For the strata consisting of herbs, low shrubs and trees <1 m tall, as well as for the strata consisting of tall shrubs and trees between 1 and 5 m, we recorded the percent of foliage consumed. In the overstory layer (i.e. intermediate trees with 5–20 m and trees taller than 20 m), we recorded the percentage of green/black/brown foliage and the trunk char height. The consensus of at least two observers was deemed necessary to validate a measurement (De Santis and Chuvieco, 2007). We calculated site CBI (i.e. overall CBI of the plot) as the average of the rating scores across all strata, vegetation CBI same as site CBI excluding the substrate, and soil CBI by averaging only the rating scores in the substrate. Categorized fire severity data was obtained through the CBI thresholds suggested by Miller and Thode (2007): low (CBI < 1.25), moderate (1.25 ≤ CBI ≤ 2.25) and high (CBI > 2.25). We used these CBI thresholds because they are widely accepted worldwide (e.g. Miller et al., 2009; Kane et al., 2014; Parks et al., 2014; Parker et al., 2015; Stambaugh et al., 2015), and provided comparable fire effects in the plant communities at the study site with those described by Miller and Thode (2007), as in other Mediterranean communities (Quintano et al., 2015, 2017; Fernández-Guisuraga et al., 2023).

2.2. Multispectral and hyperspectral satellite data

The multispectral push-broom sensor onboard Sentinel-2 satellite of the European Space Agency (ESA) provides 13 bands at different spatial resolution (10 m, 20 m, 60 m) spanning the visible-near infrared (VNIR; 10 bands) and the short-wave infrared (SWIR; 3 bands) regions. We selected a post-fire Sentinel-2A Level 2A scene covering the study site on July 15th, 2022 from the Copernicus Open Access Hub. This acquisition date was selected based on the availability of cloud-free imagery as close as possible to both field sampling and on-demand acquisition date of the cloud-free PRISMA scene. Level 2A corresponds to a bottom-of-atmosphere (i.e. surface reflectance) orthorectified product corrected for atmospheric effects by the provider using the Sen2Cor algorithm (ESA, 2022). The nearest neighbor resampling technique was used to downsample 10-m bands to a spatial resolution of 20 m. The bands at 60 m were discarded from subsequent analyses because they are heavily influenced by atmospheric effects (Jia et al., 2016).

PRISMA is the spaceborne hyperspectral mission of the Italian Space Agency (ASI) launched in March 2019, with an expected mission lifetime of 5 years. The satellite has a revisit time of 29 days at nadir viewing, and features a swath width of 30 km. The push-broom VNIR and SWIR spectrometers acquire spectral data in 240 bands between 400 and 2500 nm with a bandwidth lower than 15 nm (Cogliati et al., 2021), and at a spatial. Resolution of 30 m. On-demand acquisition of the PRISMA scene covering the study site was obtained on July 13th, 2022 under clear-sky conditions. The scene was processed by the PRISMA mission ground processor and the Level 2D product was downloaded from the mission server (https://prisma.asi.it/). Level 2D corresponds to a bottom-of-atmosphere orthorectified product corrected for atmospheric effects by the image provider using MODTRAN6 radiative transfer code (ASI, 2020; Pignatti et al., 2022). We stacked VNIR and SWIR bands to build the hyperspectral cube, keeping the SWIR bands in the spectral range where VNIR and SWIR bands overlap. The bands with artifacts and a low signal-to-noise ratio identified by visual inspection, and those in the main water vapor absorption regions, were excluded (Tane et al., 2018; Amici and Piscini, 2021) for subsequent analyses. These were bands spanning wavelengths from 400 to 434 nm, 1345–1459 nm, 1774–1975 nm, 2010–2035 nm and 2469–2505 nm. The scene presented an across-track strip with anomalous reflectance data due to a calibration failure, affecting some VNIR bands and all SWIR bands, and was consequently discarded. The strip coincided with the central axis of the wildfire but not with any CBI plot.

2.3. MESMA procedure

Two steps were followed to apply the MESMA algorithm to the original Sentinel-2 and PRISMA surface reflectance images and retrieve cover fraction images. First, endmember spectra were identified and a spectral library was built. This stage is a key step, as the adequate selection of the endmembers and their spectral signature determines the accuracy of results (Tompkins et al., 1997). Second, the spectral unmixing of the surface reflectance images was carried out using the spectral library previously defined to obtain a fraction image for each considered endmember.

2.3.1. Definition of the spectral library

The definition of the final spectral library of the land covers present in the study site consisted on the following steps:

1. Extraction of candidate endmembers from the original image (image endmembers)

This step was carried out manually using a spectral signature viewer and, according to previous fire severity studies (Quintano et al., 2013, 2017, 2020), we chose char, photosynthetic vegetation (PV), non-photosynthetic vegetation (NPV), soil, and water as endmembers to unmix the images. Based on Dudley et al. (2015) and Fernández-Manso et al. (2016b), regions of interest or georeferenced polygons of each selected class were delineated to define all candidate spectra. These polygons were homogeneous areas formed by an expected single land cover, from which the candidate spectra were extracted to create the initial spectral library. They were the same for both post-fire images (PRISMA and Sentinel-2). Delineation of polygons outside the fire scar was assisted using as reference the Spanish Forest Map, 50-cm orthophotos from Spanish Aerial Ortho-photography National Plan (PNOA) and the color composite of original images.

Spectral signature of the candidate endmembers was reviewed to verify that they had the typical shape for the analyzed targets following Quintano et al. (2020). Endmember spectra for dry grasslands lacked the typical lignocellulose absorption features centered around 2100 and 2300 nm (Fig. 2) and the sharp increase in red edge reflectance expected from own knowledge, ECOSTRESS spectral libraries (Meerdink et al., 2019) and previous research (e.g. Boelman et al., 2011; Dennison et al., 2019). This behavior may be attributable to the pronounced spatial heterogeneity of non-irrigated, dry grasslands in the study site. These communities are encroached by scattered woody vegetation, as in other Mediterranean grasslands (e.g. Maestre et al., 2011), feature a high percentage of bare soil, and commonly have wide, man-made stone walls (Peco et al., 2012) to delimit small fields. Then, the acquisition of pure pixels in these communities is almost impossible at the spatial resolution of PRISMA and a land cover aggregation effect of mixed pixels can be expected (Fernández-Guisuraga et al., 2021b), and thus

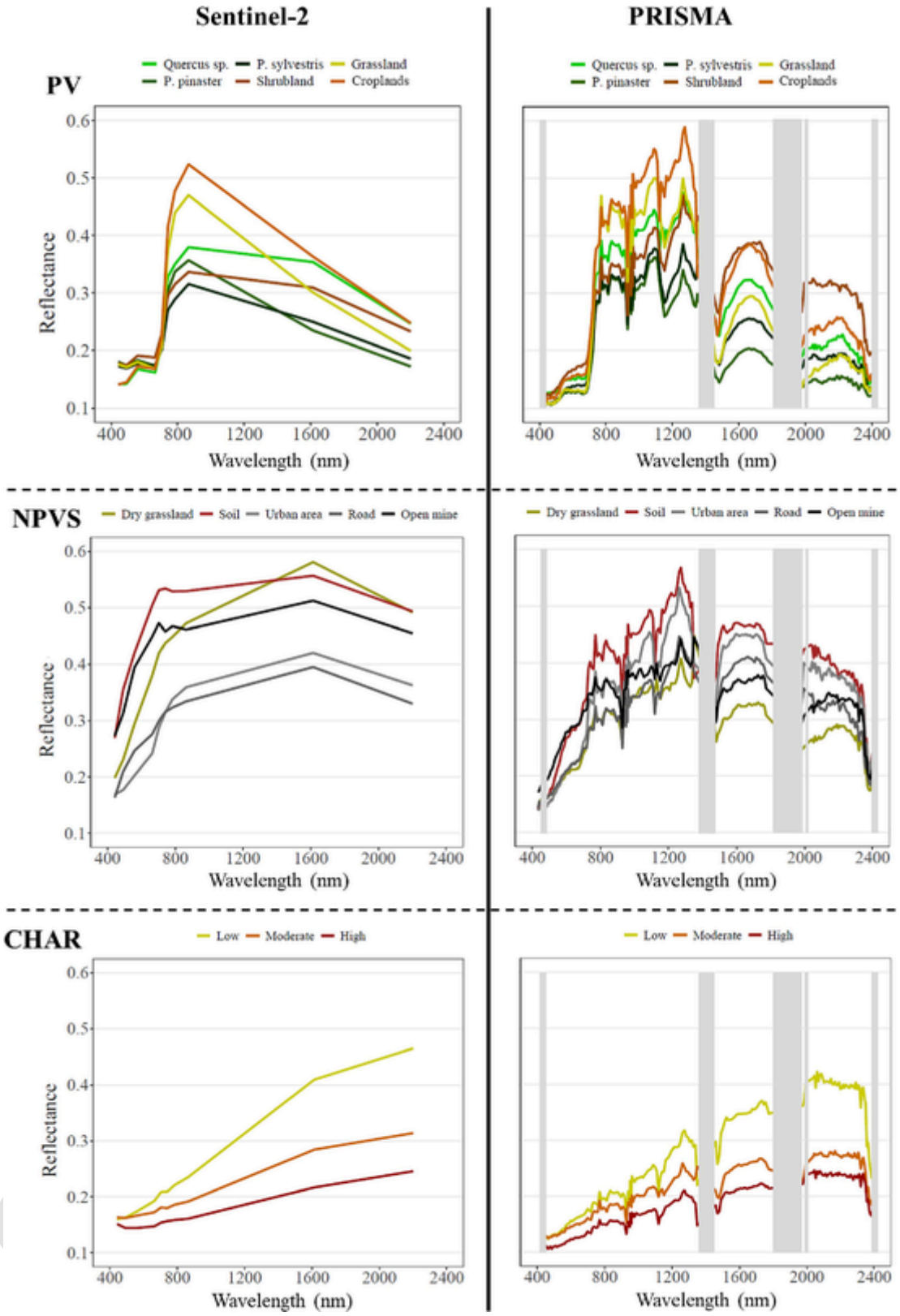

Fig. 2. Examples of endmember spectra included in the spectral library for unmixing Sentinel-2 (left) and PRISMA (right) images (PV: Photosynthetic vegetation; NPVS: Non-photosynthetic vegetation and soil). Gray shaded bands in the PRISMA plots indicate regions with artifacts, low signal-to-noise ratio or water vapor absorption.

differences in endmember spectra. Our dry grasslands' endmember spectra closely resemble the non-irrigated lands' NPV spectra used to unmix an EO-1 Hyperion image in Mediterranean communities of eastern Spain (Fernández-Manso et al., 2019). However, the impact in the unmixing result is expected to be minimal because image endmembers are collected at the same scale as the image and are easier to associate with image features (Franke et al., 2009).

Finally, char spectra were obtained from expected homogeneous polygons delineated exclusively within the fire scar, based on the color composite and their spectral signature. Char polygons were delineated in areas with different fire severity levels (low, moderate and high) to improve char fraction retrieval according to Quintano et al. (2020) and Fernández-Manso et al. (2016b, 2019).

2. Definition of the final spectral library

A semi-automatic procedure consisting of two steps was used to select the endmembers definitively included in the final spectral library following Quintano et al. (2020):

a) Iterative Endmember Selection method (IES), proposed by Schaaf et al. (2011) and updated by Roth et al. (2012). IES automatically selected the most representative endmembers of the different spectral classes based on the maximization of the classification accuracy measured by the kappa statistic. In this way, a provisional spectral library was procured.

b) Joint calculation of three indices for each candidate endmember present in the initial spectral library: (i) Endmember Average RMSE (EAR; Dennison and Roberts, 2003), which identifies endmembers that minimize RMSE within a class, and, therefore, the optimal endmember would be the one that produces the lowest EAR value; (ii) Minimum Average Spectral Angle (MASA; Dennison et al., 2004), which identifies endmembers with the minimum average spectral angle, and thus lower MASA values are preferred; and (iii) Count-based Endmember Selection Index (CoB; Roberts et al., 2003), which identifies endmembers that model the maximum number of endmembers within their class. Higher CoB values are preferred. Each index provides unique information to determine which spectra are more representative of their class while covering the most within-class variability (Roberts et al., 2019). Those endmembers not selected by the automatic IES procedure, but whose EAR, MASA and CoB index values reflected a high suitability according to Quintano et al. (2013, 2020), were manually added to the provisional spectral library to form the final spectral library. Specifically, we included an additional endmember per class based on these three indices if it jointly exhibits the highest CoB value, the lowest EAR value, and the lowest MASA value.

Endmember extraction and the definition of the spectral library were performed by using the Visualization and Image processing for Environmental Research (VIPER) tools 2.1 software (Roberts et al., 2019) (https://sites.google.com/site/ucsbviperlab/viper-tools).

2.3.2. Unmixing

Endmembers of the spectral library were organized hierarchically at different levels enabling the definition of several levels of complexity that can be used simultaneously to unmix the PRISMA and Sentinel 2 images using the multilevel fusion procedure (Roberts et al., 2003). Furthermore, once the level or levels of complexity used for unmixing were defined, we selected the maximum number of endmembers to be used in each model, as well as their specific signatures. We also adjusted the values of some restrictions used in the unmixing process: (i) maximum and minimum admissible fraction values, (ii) minimum and maximum allowable shade fraction values, (iii) maximum allowed RMSE, and (iv) maximum percentage of unclassified pixels after unmixing admissible for the results to be considered valid. The considered values were similar to those used in previous studies (Fernández-Manso et al., 2016a, 2019; Quintano et al., 2013, 2020). In particular, minimum and maximum admissible fraction values, −0.10 and 1.10, respectively; minimum and maximum allowable shade fraction values, 0.00 and 1.00, respectively; maximum allowed RMSE, 0.025; and maximum percentage of unclassified pixels, 5%. Furthermore, to minimize the influence of external factors when comparing the behavior of the two sets of fraction images (Sentinel-2 and PRISMA) in relation to CBI values, it was sought that the parameters used to perform the unmixing of the two images were the same.

Pixel unmixing is an iterative process since it may be necessary to adjust the hierarchical level of the spectral library and the number of endmembers until the imposed restrictions (i.e. admissible fraction values, allowable shade fraction values, maximum allowed RMSE and maximum percentage of unclassified pixels) are fulfilled. From this point, the definitive fraction images were shade-normalized, highlighting the contribution of the rest of the endmembers (Rogan and Franklin, 2001; Roberts et al., 2019). Finally, the cover by image fractions was extracted for each CBI plot of 30 m × 30 m by averaging the values of a regular grid of points with a 5-m spacing (Picotte and Robertson, 2011) due to the allocation of several pixels within each plot.

All procedures to unmix both post-fire images were completed by using the Visualization and Image processing for Environmental Research (VIPER) tools 2.1 software (Roberts et al., 2019) (https://sites.google.com/site/ucsbviperlab/viper-tools).

2.4. Data analyses

The relationship between the CBI (site, vegetation and soil) measured in the field plots on a continuum scale (dependent variable) and the cover by image fractions -char, PV, NPVS- (independent variables) retrieved from Sentinel-2 and PRISMA images was assessed through Random Forest regression (RFR; Breiman, 2001) ensemble learning algorithm. We chose RFR for its ability to efficiently handle overfitting issues and unravel complex interactions and non-linear relationships between predictors and with the response variable (Breiman, 2001; Cutler et al., 2007; Rodriguez-Galiano et al., 2012; Gigović et al., 2019). The *ntree* RFR model parameter was set to 2000 to guarantee stable predictions (Probst and Boulesteix, 2018), and the *mtry* parameter was tuned to find the appropriate value (*mtry* = 2). The increase in mean square error (%IncMSE) attribute was used to assess the relative importance of each independent variable in the model. We fitted separate models for Sentinel-2 and PRISMA images, both for the entire study site and also by plant community. RFR performance was assessed using 5-fold cross validation resampling, repeated 5 times, computing the average prediction across resamples. We assessed the relationship between observed and predicted CBI values using the coefficient of determination (R^2), the mean bias error (MBE), the RMSE, and the normalized RMSE (nRMSE) because of the different fire severity intervals observed in each CBI level and in each plant community. The nRMSE was computed using the difference between the maximum and minimum observed CBI values as normalizing factor (Zambrano-Bigiarini, 2020).

Ordinal Forests (OF; Hornung, 2020), a novel Random Forest-based classification algorithm adapted for ordinal responses, was used to classify categorized site CBI data (dependent variable) using the cover by image fractions -char, PV, NPVS- retrieved from Sentinel-2 and PRISMA images (independent variables). This algorithm was chosen to avoid the loss of information associated to the ordinal character of the response variable (low, moderate and high CBI) (Fernández-Guisuraga et al., 2021c), and to follow a similar modeling scheme, with comparable strengths, as for the continuum CBI. The optimal values for OF algorithm hyperparameters ($B_{sets} = 2150$, $B_{bestsets} = 10$, $B_{ntreeprior} = 150$, $B_{ntree} = 2400$, $N_{perm} = 500$) were determined through tuning experiments. See Hornung (2020) for a detailed description of the effect of hyperparameters in OF models. We selected an equal performance function to classify observations from each category with the same accuracy

independently of category sizes (Hornung, 2020). OF classification performance was evaluated using 5-fold cross validation resampling, repeated 5 times, computing the average confusion matrix across resamples. We considered the following accuracy metrics: overall accuracy (OA; %), Kappa index, and user's (UA) and producer's (PA) accuracy (%) for each class.

RF and OF analyses were conducted in R (R Core Team, 2021) using the "randomForest" (Liaw and Wiener, 2002), "ordinalForest" (Hornung, 2022) and "caret" (Kuhn, 2020) packages.

3. Results

The endmembers extracted from the Sentinel-2 and PRISMA surface reflectance images included several classes representative of the study site (Table 1 level 1 column). Based on previous studies (Quintano et al., 2013, 2020; Fernández-Guisuraga et al., 2022), five hierarchical levels were established in the spectral library from the land cover by grouping the level 1 classes (Table 1). The joint use of the automatic IES algorithm and the EAR, MASA and CoB indices enabled the identification of the optimal spectra for building the final spectral library. Some examples of the endmember spectra included in the final spectral library are displayed in Fig. 2. The number of endmembers of each class (level 1) was similar for Sentinel-2 and PRISMA images (Table 2).

It must be emphasized that, as indicated in the Section 2.3.2, before the definitive fraction images were calculated several unmixing trials were performed by varying the hierarchical level of the spectral library and the number of included endmembers. In our study, the highest percentage of Sentinel-2 and PRISMA classified pixels after unmixing was achieved by using the hierarchical level 3, with 3- and 4-endmember models, and including all the endmembers of the final spectral library except those corresponding to the water class. Thus, to calculate the definitive fraction images we tested 1378 and 1386 3-endmembers models, and 9576 and 9720 4-endmembers models for the Sentinel-2 and PRISMA images, respectively. However, the number of models finally used for the Sentinel-2 and PRISMA images was 6598 and 3223, respectively, which represents approximately 60% and 30% of the models tested.

The percentage of unclassified pixels was 1.45% in the PRISMA scene and 0.82% in the Sentinel-2 scene (Table 3), respectively, numbers much lower than the threshold proposed by literature (5%; Quintano et al., 2017). The percentage of pixels unmixed by 3- and 4-endmember models that included the char endmember in the PRISMA scene (38.05%) was slightly higher than in the Sentinel-2 scene (35.79%) (Table 3).

The shade-normalized char fraction images for Sentinel-2 and PRISMA scenes (Fig. 3) clearly discriminated burned from unburned areas inside and outside the fire perimeter, but the Sentinel-2 char fraction showed higher noise corresponding to unburned areas. Differences in char, PV and NPVS fraction values within the fire perimeter suggest different fire severity levels (Fig. 3).

The mean site CBI (i.e. overall CBI of each plot) within the fire scar was equal to 1.89. 20% of the plots were classified as low severity (CBI < 1.25), 40% as moderate severity (1.25 ≤ CBI ≤ 2.25) and 40% as high severity (CBI > 2.25). Maritime pine stands featured the highest fire severity, with a mean site CBI equal to 2.32. The lowest fire severity was registered in Pyrenean oak forests (mean site CBI equal to 1.55), according to expectations. The mean vegetation and soil CBI within the fire scar were equal to 2.10 and 1.69, respectively.

The accuracy of the RFR models trained with PRISMA fraction images (char, PV and NPVS) used to retrieve site, vegetation and soil fire severity (R^2 = 0.64–0.79 and RMSE = 0.33–0.41) was substantially higher than that achieved from Sentinel-2 (R^2 = 0.27–0.53 and RMSE = 0.54–0.60) based on field-based fire severity assessments for the entire study area (Fig. 4). For both sensors, the lowest performance was obtained in the retrieval of soil fire severity, although the differ-

Table 1
Hierarchical levels of multiple endmember spectral mixture analysis (MESMA) spectral library.

Level 1	Level 2	Level 3	Level 4	Level 5
Woodlands of *Quercus* sp.	PV	PV	PV	VSW
Forests of *Pinus pinaster*				
Forests of *Pinus sylvestris*				
Shrublands				
Grasslands				
Irrigated croplands				
Dry grasslands	NPV	NPVS	NPVSW	
Soil	Soil			
Urban areas				
Roads				
Open mine				
Dam	Water	Water		
River				
High fire severity	Char	Char	Char	Char
Moderate fire severity				
Low fire severity				

PV: Photosynthetic vegetation; NPV: Non-photosynthetic vegetation; NPVS: Non-photosynthetic vegetation and soil; NPVSW: Non-photosynthetic vegetation, soil and water; VSW: vegetation, soil and water

Table 2
Number of endmembers of the definitive spectral library.

Levels 1&2 of spectral library	#Endmembers	
	PRISMA image	Sentinel 2 image
PV	**27**	**28**
Woodlands of Quercus spp.	6	5
Forests of Pinus pinaster Ait.	3	3
Forests of Pinus sylvestris L.	4	4
Shrublands	4	5
Grasslands	5	6
Irrigated croplands	5	5
NPV	**8**	**7**
Dry grasslands	8	7
Soil	**12**	**12**
Soils	4	4
Urban areas	4	4
Roads	3	3
Open mine	1	1
Water	**6**	**3**
Dam	4	2
River	2	1
Char	**19**	**18**
High fire severity	11	11
Moderate fire severity	4	4
Low fire severity	4	3

PV: Photosynthetic vegetation; NPV: Non-photosynthetic vegetation

Table 3
Summary of unmixing results in terms of number of pixels classified by 3- and 4-endmember models in the hierarchical level 3.

Model Complexity	Hierarchical level 3	%Classified pixels	
		PRISMA	Sentinel 2
3-endmember models	CHAR – PV - shade	10.13	8.48
	CHAR – NPVS - shade	25.96	23.75
	PV – NPVS - shade	60.98	63.39
	Total 3-endmember models	**97.07**	**95.62**
4-endmember models	CHAR – PV – NPVS - shade	1.46	3.56
	Total 4-endmember models	**1.46**	**3.56**
Total classified		**98.53**	**99.18**
Unclassified		**1.47**	**0.82**
TOTAL		**100**	**100**

PV: Photosynthetic vegetation; NPVS: Non-photosynthetic vegetation and soil

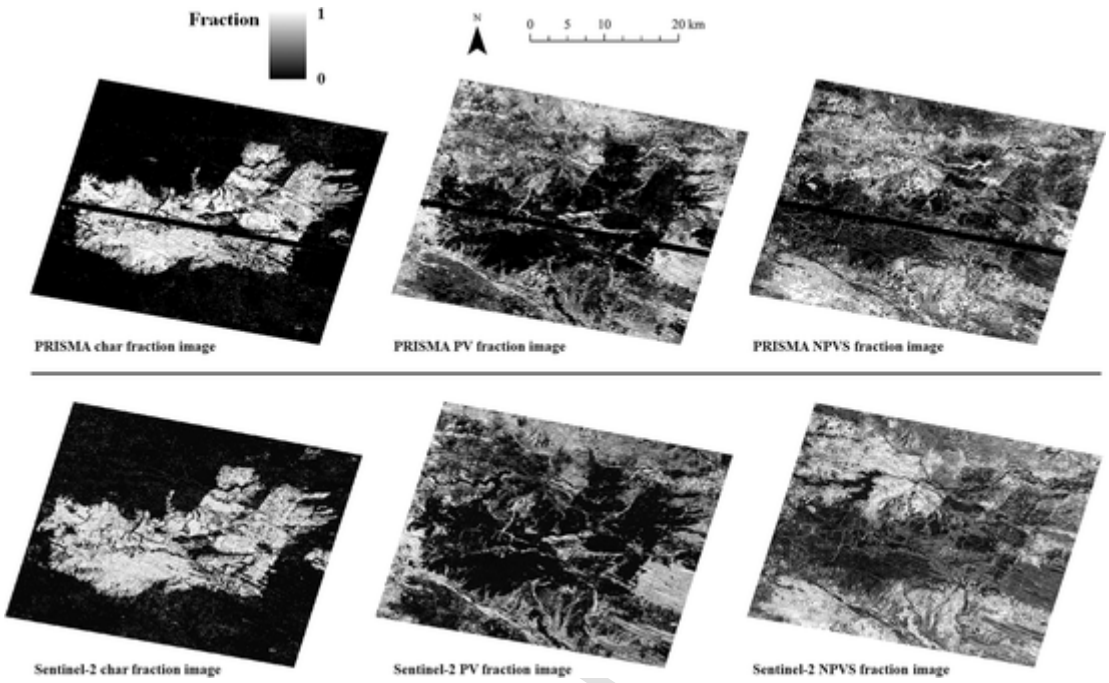

Fig. 3. Shade-normalized fraction images from Multiple Endmember Spectral Mixture Analysis (MESMA) procedure (PV: Photosynthetic vegetation; NPVS: Non-photosynthetic vegetation and soil).

ence in retrieval performance between vegetation/site and soil fire severity was lower in the case of PRISMA. Fire severity was slightly underestimated for high field-measured severity values (CBI > 2.25) from the Sentinel-2 retrieval, this effect being much less noticeable in the case of the PRISMA retrieval as evidenced by the MBE metric (Fig. 4). The char fraction was the most contributing variable in the RFR models (Table 4).

The performance of fire severity retrievals by plant community followed the same pattern as for the entire study site (Table 5). The retrieval from PRISMA fraction images presented a lower error (nRMSE = 13.3%–29.1%) than the Sentinel-2 retrieval (nRMSE = 18.2%–38.7%) in all communities. In general, the retrieval error was higher in Pyrenean oak and maritime pine stands (Table 5).

The spatially-explicit fire severity maps computed from RFR model outputs for PRISMA (Fig. 5) revealed that the highest fire severities occurred in the southwesternmost sector of the wildfire, spatially coincident with maritime pine plantations. In these areas, fire severity was clearly underestimated by the Sentinel-2 retrieval in concordance with field-based validation results (Fig. 4).

When considering categorized fire severity data (Table 6), the highest classification performance was also achieved by the OF model trained with PRISMA fraction images (OA = 83% and Kappa = 0.73), with Sentinel-2 obtaining modest results (OA = 57% and Kappa = 0.33). In the PRISMA-based classification, PA and UA values for each fire severity category were highly balanced and consistent with OA. Specifically, PA and UA values were always higher than 70%, including for the moderate fire severity category. In the case of Sentinel-2, high fire severity had the highest PA and UA values.

4. Discussion

Previous studies reported the potential of narrowband hyperspectral remote sensing data collected by airborne or the technology-demonstrator Hyperion spectrometers to produce meaningful, physically-based estimates of fire severity through the fractional cover retrieval of representative ground components in a post-fire landscape (Lewis et al., 2007, 2011; Veraverbeke et al., 2014; Fernández-Manso et al., 2019). Nevertheless, these findings are limited by the low ability to evaluate large surfaces and high costs of airborne acquisitions (Veraverbeke et al., 2018), as well as the low signal-to-noise ratio and narrow swath width of Hyperion scenes (Papeş et al., 2010). A key finding of this study is that state-of-the-art PRISMA spaceborne spectrometer overcomes these limitations in the context of extreme wildfire events. First, the on-demand acquisition of PRISMA scenes is straightforward as compared to airborne hyperspectral data (Veraverbeke et al., 2014). Second, the PRISMA retrieval performance of sub-pixel components directly related to fire severity was remarkably high in spite of the lower spatial resolution than airborne spectrometers, and in line with previous research involving airborne hyperspectral data (e.g. Lewis et al., 2011; Veraverbeke et al., 2014).

The basis of the proposed fire severity assessment with PRISMA hyperspectral data, benchmarked with the multispectral capabilities of Sentinel-2, relied on the representative characterization of per-pixel fractional cover in the post-fire scenes. The high classification percentage (> 98.5%) of PRISMA and Sentinel-2 scenes could be accounted for by the precise endmember selection through the combination of the IES algorithm with EAR, MASA and CoB indices (Quintano et al., 2020), avoiding ill-posed models and data overfitting (Li et al., 2005). Fernández-Manso et al. (2019) and Quintano et al. (2020) achieved similar unmixing percentages when using a multi-level fusion approach and comparable hierarchical levels of the spectral library to retrieve post-fire fractional covers from Hyperion and Sentinel-2 scenes, respectively. Here, NPV and soil formed just one category in the third level of the spectral library. This finding agrees with previous studies suggesting that the grouping of NPV and soil in a unique spectral library (NPVS) provided accurate results in the classification of burned landscapes (Fernández-Manso et al., 2019; Quintano et al., 2017; Quintano et al., 2019). The fewer potential MESMA models required by the PRISMA scene for subpixel fraction estimation than the Sentinel-2 scene may be associated with the increased spectral data volume of PRISMA, and thus the improved capture of distinctive spectral features within classes (Lewis et al., 2011; Degerickx et al., 2019). This may also explain both the high number of unmixed pixels that included a char end-

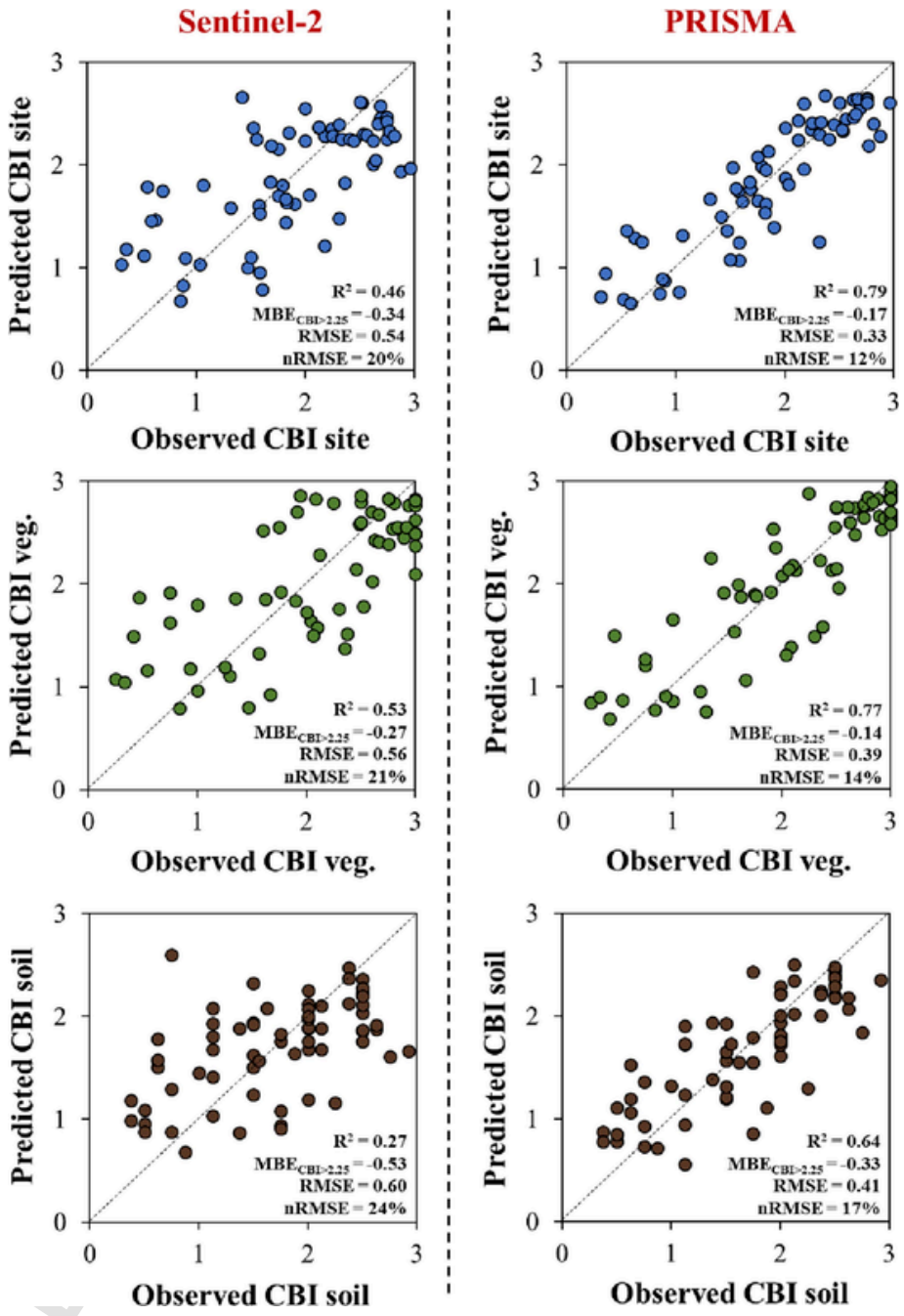

Fig. 4. Relationship between observed and predicted site, vegetation and soil Composite Burn Index (CBI) for the Sentinel-2 and PRISMA retrievals considering all plant communities together.

member and the low char fraction noise from the PRISMA post-fire scene.

Fire severity retrieval in a continuum scale from PRISMA post-fire fraction images outperformed the Sentinel-2 retrieval at the site, vegetation and soil levels in our study. PRISMA retrieval accuracies reported here, attributable to high spectral resolution and spectral data dimensionality (van Wagtendonk et al., 2004; Veraverbeke et al., 2014, 2018; Fernández-Manso et al., 2019), are comparable to previous studies using a variety of airborne hyperspectral sensors and SMA-based approaches, including MESMA. For example, Veraverbeke et al. (2014) found that the burned fraction retrieved from AVIRIS data had higher correlation with the geometrically structured CBI (GeoCBI; R^2 = 0.86) than Landsat OLI-based estimates (R^2 = 0.65) over the Canyon Fire (California, United States). In the Taylor Complex fires occurred in Alaska's boreal forest, Lewis et al. (2011) evidenced varying correlations (R^2 = 0.27–0.79) between PV and char fraction images retrieved from HyMap hyperspectral data, and post-fire ground components measured in the field. Robichaud et al. (2007) found moderate to strong correlations (R^2 = 0.21 to 0.48) between field-measured fractional cover of ash, soil, and vegetation and that retrieved from Probe I hyperspectral sensor in the Hayman wildfire in the Rocky Mountains. Despite the higher spatial resolution procured by airborne hyperspectral sensors (Lewis et al., 2007), this may not be a decisive parameter at the scale of CBI plots in view of the accuracies obtained in this study at moderate spatial resolution.

A plausible explanation for the enhanced retrieval performance of site and vegetation fire severity compared to that of soil may be related to the occlusion of background signal by vegetation legacies and burned

Table 4
Variable importance in Random Forest regression (RFR) models for site, vegetation and soil Composite Burn Index (CBI), measured as the percentage increase in mean square error (%IncMSE).

%IncMSE		CBI components		
		site	vegetation	soil
Sentinel-2	**Char**	57.83	56.42	48.21
	PV	24.20	27.96	18.36
	NPVS	18.54	25.28	12.58
PRISMA	**Char**	60.79	63.11	54.49
	PV	33.27	35.99	26.43
	NPVS	36.13	32.35	35.23

PV: Photosynthetic vegetation; NPVS: Non-photosynthetic vegetation and soil

Table 5
Random Forest regression (RFR) model performance for each plant community, assessed through the normalized RMSE (nRMSE). Errors above 25% are displayed in red.

nRMSE (%)		CBI components		
		site	vegetation	soil
Sentinel-2	Holm oak	**25.1**	24.4	24.8
	Pyrenean oak	**26.9**	**27.2**	**37.5**
	Maritime pine	**38.4**	**38.7**	**32.8**
	Scots pine	19.1	20.0	24.5
	Shrub	18.2	18.6	20.9
PRISMA	Holm oak	21.1	22.1	21.2
	Pyrenean oak	19.6	24.2	**28.7**
	Maritime pine	22.3	**29.1**	24.4
	Scots pine	15.0	13.5	20.9
	Shrub	13.3	14.6	13.9

remnants (Fernández-García et al., 2018a), especially in areas burned at low or moderate fire severity, where the overstory strata are most closely related to plot reflectance (Hudak et al., 2007; Cansler and McKenzie, 2012). However, the loss of performance in the retrieval of soil fire severity was less pronounced in the case of PRISMA (≈ 29%) than in Sentinel-2 (≈ 55%) estimates, most probably associated with the fire-amplified spectral similarities in forest background materials in the band configuration of multispectral sensors (Robichaud et al., 2007; Finley and Glenn, 2010; Peón et al., 2017). Nevertheless, the accuracy of the PRISMA-based soil fire severity retrieval was remarkably high (R^2 = 0.63). The char fraction featured the highest importance in all fire severity retrievals, in line with previous studies that reported the relevance of the char fraction as a site fire severity indicator (Quintano et al., 2017; Tane et al., 2018; Fernández-Manso et al., 2019). Here, we also evidenced that char fraction was the most important post-fire ground constituent on individual vegetation and soil severity assessments.

The underestimation of high fire severity was minimal in PRISMA estimates compared to those of Sentinel-2, which could be related with the suboptimal sensitivity of Sentinel-2 discrete SWIR bands to soil and char cover (Roy et al., 2006; Lentile et al., 2009), and also to SWIR reflectance saturation at high CBI values (Soverel et al., 2010). The performance of fire severity estimates from both sensors decreased, particularly Sentinel-2, in communities dominated by maritime pine and Pyrenean oak, with CBI values measured in the field plots between 1.5 and 3 and 0.5–2, respectively. The lower performance may have been driven by the narrow range of fire severity in both communities (Allen and Sorbel, 2008), but also by decoupled canopy and surface fire effects (Saberi et al., 2022). In fact, maritime pine stands and mature Pyrenean oak communities showed the greatest difference in mean vegetation and soil fire severity values (≈ 0.75 CBI units).

The normalized error in the fire severity retrieval considering a continuum CBI scale was below 25% when we pooled all communities together for both sensors, which is considered an acceptable accuracy

Fig. 5. Composite Burn Index (CBI) maps computed from Random Forest regression (RFR) model outputs for Sentinel-2 and PRISMA.

Table 6
Ordinal Forests (OF) classification performance evaluated through the average confusion matrix computed across 5-fold cross validation resamples.

Sentinel-2		Reference fire severity		
		Low	Moderate	High
Classified fire severity	Low	10.6	11.4	1.1
	Moderate	5.7	11.4	4.3
	High	2.3	19.4	33.7
	PA (%)	57.90	26.83	87.18
	UA (%)	47.83	52.38	61.82
	OA (%)	**Kappa**		
	56.57	0.33		
PRISMA		**Reference fire severity**		
		Low	Moderate	High
Classified fire severity	Low	17.2	5.2	0.9
	Moderate	1.2	31.3	1.8
	High	0.0	8.2	34.2
	PA (%)	94.44	70.46	91.89
	UA (%)	73.91	91.18	80.95
	OA (%)	**Kappa**		
	82.83	0.73		

OA: overall accuracy; UA: user's accuracy; PA: producer's accuracy

threshold in fire severity assessment (e.g. De Santis and Chuvieco, 2007; Fernández-García et al., 2018a). However, only PRISMA-based estimates remained below 25% for the site CBI when the analysis is stratified by plant community. Going one step further by considering categorized fire severity data using the thresholds proposed by Miller and Thode (2007), we found that PRISMA-based classification enabled

highly accurate fire severity estimates, with consistent PA and UA values for each fire severity class. We can suggest that the introduction of hyperspectral data unmixing, particularly in a wildfire with large sections burned at moderate fire severity, solved to a large extent the high confusion between moderate and low/high fire severity categories (Miller and Thode, 2007). This problem is typical when unmixing broadband data (Quintano et al., 2013; Quintano et al., 2017), and was also evidenced in this study. In this sense, PRISMA data volume was able to spectrally resolve the alternate fire effects that define the complex nature of areas burned at moderate or mixed severity (Miller et al., 2009).

Altogether, the results of this study are significantly relevant to the fire ecology field, even more so considering the recent, and increasing availability of spaceborne hyperspectral missions besides PRISMA, such as Earth Sensing Imaging Spectrometer (DESIS) and Hyperspectral Imager Suite (HISUI) onboard International Space Station (ISS), EnMAP, or AHSI onboard GF-5 satellite, and upcoming NASA Surface Biology and Geology (SBG) and Copernicus Hyperspectral Imaging Mission for the Environment (CHIME) missions. Nevertheless, we are also aware of several limitations of this study. First, PRISMA and Sentinel-2 scenes were atmospherically corrected using different algorithms already implemented by the image provider. We chose vendor-supplied surface reflectance products to minimize image processing workflows in a potential operational-use context in fire severity assessments. We assume that slight differences could exist in the reflectance output of the atmospheric correction algorithms, but no significant implications for our analyses are expected as in previous studies (Quintano et al., 2018; Cardille et al., 2022; Johnson and Mueller, 2021). Additionally, we used image endmembers to form the MESMA spectral library independently for each sensor and thus the impact of atmospheric correction is minimized. Second, our study is based on a single fire event and the transferability of the methodological approach should be further tested in other Mediterranean ecosystems and biomes to evaluate the potential of new spaceborne hyperspectral missions for regional to global fire severity assessments. However, the fire is extensive (28,046 ha) and the land cover is heterogeneous since different Mediterranean plant communities are encompassed within the fire scar, our PRISMA-based approach featuring a remarkable performance in each community. Moreover, the physical basis of MESMA has proven to show an adequate generalization ability in burned landscapes (e.g. Fernández-Guisuraga et al., 2022). Third, the number of field plots could have been higher but we decided to minimize the time lag between the end of the field sampling campaign and the date of the PRISMA on-demand image acquisition. Likewise, the field sampling campaign had to be completed before the burned wood extraction by the Regional Forest Service. We did not consider control CBI plots because unburned areas within the fire scar were dominated by residential fuels and agricultural lands in wildland-urban interfaces, as well as riparian vegetation in valley-bottoms. Unburned islands with the presence of representative Mediterranean plant communities were very small and located between low severity areas. Accordingly, their size and shape were not adequate enough to accommodate homogeneous CBI plots. Presumably, the use of control CBI plots may have decreased the precision of the fire severity estimates, which is more realistic as there is potential confusion between unburned and low fire severity areas (McCarley et al., 2018). However, these areas are not a priority for the implementation of post-fire emergency management (De Santis et al., 2009). Despite the promising results involving spaceborne hyperspectral data availability to assess fire severity, further research could take advantage of the on-demand scene acquisition and increased catalog availability of new spaceborne hyperspectral sensors like PRISMA to conduct multitemporal sub-pixel image analyses (Sunderman and Weisberg, 2011; Quintano et al., 2019), more ecologically linked to fire severity definition than monotemporal perspectives (Tane et al., 2018).

5. Conclusions

This study contributes to the continued efforts for evaluating the ecological effects of wildfire disturbances in fire-prone ecosystems and extends the fire severity assessments of previous studies using airborne spectrometers to the state-of-the-art spaceborne spectrometer missions. We evaluated for the first time the retrieval of sub-pixel components directly related to fire severity by leveraging the high dimensionality of hyperspectral data provided by the PRISMA mission. Our results showed that MESMA fraction images retrieved from PRISMA hyperspectral data provided reliable fire severity estimates in the line of previous studies utilizing a variety of airborne hyperspectral sensors, at the expense of less complex logistics and processing workflows than the latter. Continuum fire severity estimates using PRISMA data clearly outperformed those based on Sentinel-2, the spaceborne mission with multispectral band setting capabilities that has previously provided the most reliable results. Also, the PRISMA-based classification of fire severity was accurate and solved the typical confusion between moderate and low/high fire severity categories when using broadband multispectral data. We conclude that spaceborne spectrometer missions may provide improved insights to support adequate post-fire management strategies, but the approach followed in this study should be tested across distinct regions worldwide.

Funding

This study was carried out using a PRISMA Product © of the Italian Space Agency (ASI), delivered under an ASI License to use. This study was financially supported by the Spanish Ministry of Science and Innovation and NextGenerationEU funds, in the framework of the FIREMAP (TED2021-130925B-I00) project; by the Regional Governments of Castilla and León, in the framework of the WUIFIRECYL (LE005P20) project, and the Principality of Asturias/FICYT (AYUD/2021/51261); by the British Ecological Society in the framework of the SR22–100154 project, where José Manuel Fernández-Guisuraga is the Principal Investigator; and by the Portuguese Foundation for Science and Technology in the frame of project UIDB/04033/2020. José Manuel Fernández-Guisuraga was supported by a Ramón Areces Foundation postdoctoral fellowship.

Uncited references

CRediT authorship contribution statement

Carmen Quintano : Conceptualization, Investigation, Methodology, Formal analysis, Writing – original draft. **Leonor Calvo :** Conceptualization, Investigation, Writing – review & editing, Supervision, Project administration, Funding acquisition. **Alfonso Fernández-Manso :** Investigation, Methodology, Formal analysis, Writing – review & editing. **Susana Suárez-Seoane :** Methodology, Formal analysis, Writing – review & editing. **Paulo M. Fernandes :** Conceptualization, Formal analysis, Writing – review & editing, Project administration, Funding acquisition. **José Manuel Fernández-Guisuraga :** Conceptualization, Investigation, Methodology, Formal analysis, Writing – review & editing, Supervision.

Declaration of Competing Interest

The authors declare that they have no known competing financial interests or personal relationships that could have appeared to influence the work reported in this paper.

Data availability

Data will be made available on request.

References

Adams, J.B., Smith, M.O., Johnson, P.E., 1986. Spectral mixture modeling: a new analysis of rock and soil types at the Viking Lander 1 site. J. Geophys. Res. 91, 8098–8112.

Allen, J.L., Sorbel, B., 2008. Assessing the differenced normalized burn ratio's ability to map burn severity in the boreal forest and tundra ecosystems of Alaska's national parks. Int. J. Wildland Fire 17, 463–475.

Amici, S., Piscini, A., 2021. Exploring PRISMA scene for fire detection: case study of 2019 bushfires in ben halls gap National Park, NSW,Australia. Remote Sens. 13, 1410.

Arnan, X., Quevedo, L., Rodrigo, A., 2013. Forest fire occurrence increases the distribution of a scarce forest type in the Mediterranean Basin. Acta Oecol. 46, 39–47.

ASI, 2020. PRISMA Products Specification Document Issue 2.3 Date 12/03/2020. Available at: (Accessed 30 November 2022). http://prisma.asi.it/missionselect/docs/PRISMA%20Product%20Specifications_Is2_3.pdf.

Boelman, N.T., Gough, L., McLaren, J.R., Greaves, H., 2011. Does NDVI reflect variation in the structural attributes associated with increasing shrub dominance in Arctic Tundra? Environ. Res. Lett. 6, 035501.

Breiman, L., 2001. Random forests. Mach. Learn. 45, 5–32.

Cansler, C.A., McKenzie, D., 2012. How robust are burn severity indices when applied in a new Region? Evaluation of alternate field-based and remote-sensing methods. Remote Sens. 4, 456–483.

Cardille, J.A., Perez, E., Crowley, M.A., Wulder, M.A., White, J.C., Hermosilla, T., 2022. Multi-sensor change detection for within-year capture and labelling of forest disturbance. Remote Sens. Environ. 268, 112741.

Chuvieco, E., De Santis, A., Riaño, D., Halligan, K., 2007. Simulation approaches for burn severity estimation using remotely sensed images. Fire Ecol. 3, 129–150.

Cocks, T., Jenssen, R., Stewart, W.I., Shields, T., 1998. The HyMap airborne hyperspectral sensor: The system, calibration and performance. In: Schaepman, M., Schläpfer, D., Itten, K.I. (Eds.), Proceedings of the 1st EARSeL Workshop on Imaging Spectroscopy, EARSeL, Paris.

Cogliati, S., Sarti, F., Chiarantini, L., Cosi, M., Lorusso, R., Lopinto, E., Miglietta, F., Genesio, L., Guanter, L., Damm, A., Pérez-López, S., Scheffler, D., Tagliabue, G., Panigada, C., Rascher, U., Dowling, T.P.F., Giardino, C., Colombo, R., 2021. The PRISMA imaging spectroscopy mission: overview and first performance analysis. Remote Sens. Environ. 262, 112499.

Combal, B., Baret, F., Weiss, M., Trubuil, A., Macé, D., Pragnère, A., Myneni, R., Knyazikhin, Y., Wang, L., 2003. Retrieval of canopy biophysical variables from bidirectional reflectance: using prior information to solve the ill-posed inverse problem. Remote Sens. Environ. 84, 1–15.

Cotrufo, S., Sandu, C., Tonolo, F.G., Boccardo, P., 2018. Building damage assessment scale tailored to remote sensing vertical imagery. Eur.J.Remote Sens. 51, 991–1005.

Cutler, D.R., Edwards, T.C., Beard, K.H., Cutler, A., Hess, K.T., Gibson, J., Lawler, J.J., 2007. Random forests for classification in ecology. Ecology 88, 2783–2792.

Degerickx, J., Roberts, D.A., Somers, B., 2019. Enhancing the performance of Multiple Endmember Spectral Mixture Analysis (MESMA) for urban land cover mapping using airborne lidar data and band selection. Remote Sens.Environ. 221, 260–273.

Delcourt, C.J.F., Combee, A., Izbicki, B., Mack, M.C., Maximov, T., Petrov, R., Rogers, B.M., Scholten, R.C., Shestakova, T.A., van Wees, D., Veraverbeke, S., 2021. Evaluating the differenced normalized burn ratio for assessing fire severity using Sentinel-2 Imagery in Northeast Siberian Larch Forests. Remote Sens. 13, 2311.

De Santis, A., Chuvieco, E., 2007. Burn severity estimation from remotely sensed data: performance of simulation versus empirical models. Remote Sens. Environ. 108, 422–435.

De Santis, A., Chuvieco, E., Vaughan, P.J., 2009. Short-term assessment of burn severity using the inversion of PROSPECT and GeoSail models. Remote Sens. Environ. 113, 126–136.

De Santis, A., Asner, G.P., Vaughan, P.J., Knapp, D.E., 2010. Mapping burn severity and burning efficiency in California using simulation models and Landsat imagery. Remote Sens. Environ. 114, 1535–1545.

Dennison, P.E., Halligan, K.Q., Roberts, D.A., 2004. A comparison of error metrics and constraints for multiple endmember spectral mixture analysis and spectral angle mapper. Remote Sens. Environ. 93, 359–367.

Dennison, P.E., Roberts, D.A., 2003. Endmember selection for mapping chaparral species and fraction using Multiple Endmember Spectral Mixture Analysis. Remote Sens. Environ. 41, 123–135.

Dennison, P.E., Qi, Y., Meerdink, S.K., Kokaly, R.F., Thompson, D.R., Daughtry, C.S.T., Quemada, M., Roberts, D.A., Gader, P.D., Wetherley, E.B., Numata, I., Roth, K.L., 2019. Comparison of methods for modeling fractional cover using simulated satellite hyperspectral imager spectra. Remote Sens. 11, 2072.

Dudley, K.L., Dennison, P.E., Roth, K.L., Roberts, D.A., Coates, A.R., 2015. A multi-temporal spectral library approach for mapping vegetation species across spatial and temporal phenological gradients. Remote Sens. Environ. 167, 121–134.

Eidenshink, J., Schwind, B., Brewer, K., Zhu, Z.L., Quayle, B., Howard, S., 2007. A project for monitoring trends in burn severity. Fire Ecol. 3, 3–21.

Epting, J., Verbyla, D., Sorbel, B., 2005. Evaluation of remotely sensed indices for assessing burn severity in interior Alaska using Landsat TM and ETM+. Remote Sens. Environ. 96, 328–339.

ESA, 2022. Sentinel-2 MSI User Guide. Available at: https://sentinel.esa.int/web/sentinel/user-guides/sentinel-2-msi. Accessed 30 November 2022.

European Commission, 2022. Forest Fires in Europe, Middle East and North Africa 2021. JRC Technical Report EUR 31269 EN. ISBN 978-92-76-58585-5.

Fernandes, P.M., 2013. Fire-smart management of forest landscapes in the Mediterranean basin under global change. Landsc. Urban Plan. 110, 175–182.

Fernández-García, V., Santamarta, M., Fernández-Manso, A., Quintano, C., Marcos, E., Calvo, L., 2018. Burn severity metrics in fire-prone pine ecosystems along a climatic gradient using Landsat imagery. Remote Sens.Environ. 206, 205–217.

Fernández-García, V., Quintano, C., Taboada, A., Marcos, E., Calvo, L., Fernández-Manso, A., 2018b. Remote sensing applied to the study of fire regime attributes and their influence on post-fire greenness recovery in pine ecosystems. Remote Sens. 10, 733.

Fernández-Guisuraga, J.M., Suárez-Seoane, S., Calvo, L., 2019. Modeling Pinus pinaster forest structure after a large wildfire using remote sensing data at high spatial resolution. For. Ecol. Manag. 446, 257–271.

Fernández-Guisuraga, J.M., Suárez-Seoane, S., Calvo, L., 2021a. Radiative transfer modeling to measure fire impact and forest engineering resilience at short-term. ISPRS J. Photogramm. Remote Sens. 176, 30–41.

Fernández-Guisuraga, J.M., Verrelst, J., Calvo, L., Suárez-Seoane, S., 2021b. Hybrid inversion of radiative transfer models based on high spatial resolution satellite reflectance data improves fractional vegetation cover retrieval in heterogeneous ecological systems after fire. Remote Sens. Environ. 255, 112304.

Fernández-Guisuraga, J.M., Suárez-Seoane, S., García-Llamas, P., Calvo, 2021. Vegetation structure parameters determine high burn severity likelihood in different ecosystem types: a case study in a burned Mediterranean landscape. J.Environ.Manag. 288, 112462.

Fernández-Guisuraga, J.M., Suárez-Seoane, S., Quintano, C., Fernández-Manso, A., Calvo, L., 2022b. Comparison of physical-based models to measure forest resilience to fire as a function of burn severity. Remote Sens. 14, 5138.

Fernández-Guisuraga, J.M., Calvo, L., Quintano, C., Fernández-Manso, A., Fernandes, P.M., 2023. Fractional vegetation cover ratio estimated from radiative transfer modeling outperforms spectral indices to assess fire severity in several Mediterranean plant communities. Remote Sens. Environ. 290, 113542.

Fernández-Manso, A., Fernández-Manso, O., Quintano, C., 2016a. SENTINEL-2A red-edge spectral indices suitability for discriminating burn severity. Int. J. Appl. Earth Obs. Geoinf. 50, 170–175.

Fernández-Manso, A., Quintano, C., Roberts, D.A., 2016b. Burn severity influence on postfire vegetation cover resilience from Landsat MESMA fraction images time series in Mediterranean forest ecosystems. Remote Sens. Environ. 184, 112–123.

Fernández-Manso, A., Quintano, C., Roberts, D.A., 2019. Burn severity analysis in Mediterranean forests using maximum entropy model trained with EO-1 hyperion and LiDAR data. ISPRS J. Photogramm. Remote Sens. 155, 102–118.

Finley, C.D., Glenn, N.F., 2010. Fire and vegetation type effects on soil hydrophobicity and infiltration in the sagebrush-steppe: II. Hyperspectral analysis. J. Arid Environ. 74, 660–666.

Franke, J., Roberts, D.A., Halligan, K., Menz, G., 2009. Hierarchical Multiple Endmember Spectral Mixture Analysis (MESMA) of hyperspectral imagery for urban environments. Remote Sens.Environ. 113, 1712–1723.

Gigović, L., Pourghasemi, H.R., Drobnjak, S., Bai, S., 2019. Testing a new ensemble model based on SVM and random forest in forest fire susceptibility assessment and its mapping in Serbia's Tara National Park. Forests 10, 408.

Giorgi, F., Lionello, P., 2008. Climate change projections for the Mediterranean region. Glob. Planet. Chang. 63, 90–104.

Goetz, A.F.H., 2009. Three decades of hyperspectral remote sensing of the earth: a personal view. Remote Sens. Environ. 113, S5–S16.

Green, R.O., Eastwood, M.L., Sarture, C.M., Chrien, T.G., Aronsson, M., Chippendale, B.J., Faust, J.A., Pavri, B.E., Chovit, C.J., Solis, M., Olah, M.R., Williams, O., 1998. Imaging spectroscopy and the airborne Visible/Infrared Imaging Spectrometer (AVIRIS). Remote Sens. Environ. 65, 227–248.

Hammill, K.A., Bradstock, R.A., 2006. Remote sensing of fire severity in the Blue Mountains: influence of vegetation type and inferring fire intensity. Int. J. Wildland Fire 15, 213–226.

Harvey, B.J., Donato, D.C., Turner, M.G., 2016. Drivers and trends in landscape patterns of stand-replacing fire in forests of the US Northern Rocky Mountains (1984–2010). Landsc. Ecol. 31, 2367–2383.

Hornung, R., 2020. Ordinal forests. J. Classif. 37, 4–17.

Hornung, R., 2022. ordinalForest: Ordinal Forests: Prediction and Variable Ranking with Ordinal Target Variables. R package version 2.4-3. https://CRAN.R-project.org/package=ordinalForest.

Hudak, A.T., Morgan, P., Bobbitt, M.J., Smith, A.M.S., Lewis, S.A., Lentile, L.B., Robichaud, P.R., Clark, J.T., McKinley, R.A., 2007. The relationship of multispectral satellite imagery to immediate fire effects. Fire Ecol. 3, 64–90.

Huerta, S., Marcos, E., Fernández-García, V., Calvo, L., 2022. Resilience of Mediterranean communities to fire depends on burn severity and type of ecosystem. Fire Ecol. 18, 28.

Jia, K., Liang, S., Gu, X., Baret, F., Wei, X., Wang, X., Yao, Y., Yang, L., Li, Y., 2016. Fractional vegetation cover estimation algorithm for Chinese GF-1 wide field view data. Remote Sens. Environ. 177, 184–191.

Johnstone, J.F., Allen, C.D., Franklin, J.F., Frelich, L.E., Harvey, B.J., Higuera, P.E., Mack, M.C., Meentemeyer, R.K., Metz, M.R., Perry, G.L.W., Schoennagel, T., Turner, M.G., 2016. Changing disturbance regimes, ecological memory, and forest resilience. Front.Ecol.Environ. 14, 369–378.

Kane, V.R., North, M.P., Lutz, J.A., Churchill, D.J., Roberts, S.L., Smith, D.F., McGaughey, R.J., Kane, J.T., Brooks, M.L., 2014. Assessing fire effects on forest spatial structure using a fusion of Landsat and airborne LiDAR data in Yosemite National Park. Remote Sens. Environ. 151, 89–101.

Keeley, J.E., 2009. Fire intensity, fire severity and burn severity: a brief review and suggested usage. Int. J. Wildland Fire 18, 116–126.

Keeley, J.E., Pausas, J.G., Rundel, P.W., Bond, W.J., Bradstock, R.A., 2011. Fire as an evolutionary pressure shaping plant traits. Trends Plant Sci. 16, 406–411.

Keeley, J.E., Bond, W.J., Bradstock, R.A., Pausas, J.G., Rundel, P.W., 2012. Fire in Mediterranean Ecosystems: Ecology, Evolution and Management. Cambridge University Press, Cambridge.
Key, C.H., Benson, N., 2005. Landscape assessment: Ground measure of severity, the Composite Burn Index; and remote sensing of severity, the Normalized Burn Ratio. In: FIREMON: Fire Effects Monitoring and Inventory System (D.C. Lutes, R.E. Keane, J.F. Caratti, C.H. Key, N.C. Benson and L.J. Gangi, Eds.), USDA Forest Service, Rocky Mountain Research Station, Gen. Tech. Rep. RMRS-GTR-164, Ogden, UT. CD: LA1–LA51.
Key, C.H., 2006. Ecological and sampling constraints on defining landscape fire severity. Fire Ecol. 2, 34–59.
Kokaly, R.F., Rockwell, B.W., Haire, S.L., King, T.V.V., 2007. Characterization of post-fire surface cover, soils, and burn severity at the Cerro Grande fire, New Mexico, using hyperspectral and multispectral remote sensing. Remote Sens. Environ. 106, 305–325.
Kolden, C.A., Smith, A.M.S., Abatzoglou, J.T., 2015. Limitations and utilisation of monitoring trends in burn severity products for assessing wildfire severity in the USA. Int. J. Wildland Fire 24, 1023–1028.
Kuhn, M., 2020. caret: Classification and Regression Training. R package version 6.0-86. https://CRAN.R-project.org/package=caret.
Lasslop, G., Coppola, A.I., Voulgarakis, A., Yue, C., Veraverbeke, S., 2019. Influence of fire on the carbon cycle and climate. Curr.Clim. Change Rep. 5, 112–123.
Lazzeri, G., Frodella, W., Rossi, G., Moretti, S., 2021. Multitemporal mapping of post-fire land cover using multiplatform PRISMA hyperspectral and sentinel-UAV multispectral data: insights from case studies in Portugal and Italy. Sensors 21, 3982.
Lentile, L.B., Holden, Z.A., Smith, A.M.S., Falkowski, M.J., Hudak, A.T., Morgan, P., Lewis, S.A., Gessler, P.E., Benson, N.C., 2006. Remote sensing techniques to assess active fire characteristics and post-fire effects. Int. J. Wildland Fire 15, 319–345.
Lentile, L.B., Smith, A.M.S., Hudak, A.T., Morgan, P., Bobbitt, M.J., Lewis, S.A., Robichaud, P.R., 2009. Remote sensing for prediction of 1-year post-fire ecosystem condition. Int. J. Wildland Fire 18, 594–608.
Lewis, S.A., Lentile, L.B., Hudak, A.T., Robichaud, P.R., Morgan, P., Bobbitt, M.J., 2007. Mapping ground cover using hyperspectral remote sensing after the 2003 Simi and old wildfires in Southern California. Fire Ecol. 3, 109–128.
Lewis, S.A., Hudak, A.T., Ottmar, R.D., Robichaud, P.R., Lentile, L.B., Hood, S.M., Cronan, J.B., Morgan, P., 2011. Using hyperspectral imagery to estimate forest floor consumption from wildfire in boreal forests of Alaska, USA. Int. J. Wildland Fire 20, 255–271.
Li, L., Ustin, S.L., Lay, M., 2005. Application of multiple endmember spectral mixture analysis (MESMA) to AVIRIS imagery for coastal salt marsh mapping: a case study in China camp, CA, USA. Int. J. Remote Sens. 26, 5193–5207.
Liaw, A., Wiener, M., 2002. Classification and regression by RandomForest. R News 2, 18–22.
Lutz, J.A., van Wagtendonk, J.W., Thode, A.E., Miller, J.D., Franklin, J.F., 2009. Climate, lightning ignitions, and fire severity in Yosemite National Park, California, USA. Int. J. Wildland Fire 18, 765–774.
Maestre, F.T., Puche, M.D., Guerrero, C., Escudero, A., 2011. Shrub encroachment does not reduce the activity of some soil enzymes in Mediterranean semiarid grasslands. Soil Biol. Biochem. 43, 1746–1749.
McCarley, T.R., Smith, A.M.S., Kolden, C.A., Kreitler, J., 2018. Evaluating the mid-infrared bi-spectral index for improved assessment of low-severity fire effects in a conifer forest. Int. J. Wildland Fire 27, 407–412.
Meerdink, S.K., Hook, S.J., Roberts, D.A., Abbott, E.A., 2019. The ECOSTRESS spectral library version 1.0. Remote Sens. Environ. 230, 111196.
Meng, R., Wu, J., Schwager, K.L., Zhao, F., Dennison, P.E., Cook, B.D., Brewster, K., Green, T.M., Serbin, S.P., 2017. Using high spatial resolution satellite imagery to map forest burn severity across spatial scales in a pine barrens ecosystem. Remote Sens. Environ. 191, 95–109.
Middleton, E.M., Ungar, S.G., Mandl, D.J., Ong, L., Frye, S.W., Campbell, P.E., Landis, D.R., Young, J.P., Pollack, N.H., 2013. The earth observing one (EO-1) satellite mission: over a decade in space. IEEE J.Select.Top.Appl.Earth Observ.Remote Sens. 6, 243–256.
Miller, J.D., Thode, A.E., 2007. Quantifying burn severity in a heterogeneous landscape with a relative version of the delta normalized burn ratio (dNBR). Remote Sens. Environ. 109, 66–80.
Miller, J.D., Knapp, E.C., Key, C.H., Skinner, C.N., Isbell, C.J., Creasy, R.M., Sherlock, J.W., 2009. Calibration and validation of the relative differenced normalized burn ratio (RdNBR) to three measures of fire severity in the Sierra Nevada and Klamath Mountains, California, USA. Remote Sens. Environ. 113, 645–656.
Moreira, F., Viedma, O., Arianoutsou, M., Curt, T., Koutsias, N., Rigolot, E., Barbati, A., Corona, P., Vaz, P., Xanthopoulos, G., Mouillot, F., Bilgili, E., 2011. Landscape – wildfire interactions in southern Europe: implications for landscape management. J. Environ. Manag. 92, 2389–2402.
Johnson, D.M., Mueller, R., 2021. Pre- and within-season crop type classification trained with archival land cover information. Remote Sens. Environ. 264, 112576.
Ninyerola, M., Pons, X., Roure, J.M., 2005. AutóAtlas Climático Digital de la Península Ibérica. Metodología y aplicaciones en bioclimatología y geobotánica. Universidad noma de Barcelona. [dataset].
Norton, J., Glenn, N., Germino, M., Weber, K., Seefeldt, S., 2009. Relative suitability of indices derived from Landsat ETM + and SPOT 5 for detecting fire severity in sagebrush steppe. Int. J. Appl. Earth Obs. Geoinf. 11, 360–367.
Papeş, M., Tupayachi, R., Martínez, P., Peterson, A., Powell, G., 2010. Using hyperspectral satellite imagery for regional inventories: a test with tropical emergent trees in the Amazon Basin. J. Veg. Sci. 21, 342–354.
Parker, B.M., Lewis, T., Srivastava, S.K., 2015. Estimation and evaluation of multi-decadal fire severity patterns using Landsat sensors. Remote Sens. Environ. 170, 340–349.
Parks, S.A., Dillon, G.K., Miller, C., 2014. A new metric for quantifying burn severity: the relativized burn ratio. Remote Sens. 6, 1827–1844.
Pausas, J.G., 2004. Changes in fire and climate in the eastern Iberian Peninsula (Mediterranean basin). Clim. Chang. 63, 337–350.
Pausas, J.G., Llovet, J., Rodrigo, A., Vallejo, R., 2008. Are wildfires a disaster in the Mediterranean basin? – a review. Int. J. Wildland Fire 17, 713–723.
Pausas, J.G., Keeley, J.E., 2014. Abrupt climate-independent fire regime changes. Ecosystems 17, 1109–1120.
Peco, B., Carmona, C.P., de Pablos, I., Azcárate, F.M., 2012. Effects of grazing abandonment on functional and taxonomic diversity of Mediterranean grasslands. Agric. Ecosyst. Environ. 152, 27–32.
Peón, J., Fernández, S., Recondo, C., Calleja, J.F., 2017. Evaluation of the spectral characteristics of five hyperspectral and multispectral sensors for soil organic carbon estimation in burned areas. Int. J. Wildland Fire 26, 230–239.
Picotte, J.J., Robertson, K.M., 2011. Validation of remote sensing of burn severity in south-eastern US ecosystems. Int. J. Wildland Fire 20, 453–464.
Picotte, J.J., Bhattarai, K., Howard, D., Lecker, J., Epting, J., Quayle, B., Benson, N., Nelson, K., 2020. Changes to the monitoring trends in burn severity program mapping production procedures and data products. Fire Ecol. 16, 16.
Pignatti, S., Amodeo, A., Carfora, M.F., Casa, R., Mona, L., Palombo, A., Pascucci, S., Rosoldi, M., Santini, F., Laneve, G., 2022. PRISMA L1 and L2 performances within the PRISCAV project: the pignola test site in southern Italy. Remote Sens. 14, 1985.
Probst, P., Boulesteix, A.L., 2018. To tune or not to tune the number of trees in random forest. J. Mach. Learn. Res. 18, 1–18.
Quintano, C., Fernández-Manso, A., Fernández-Manso, O., Shimabukuro, Y.E., 2006. Mapping burned areas in Mediterranean countries using spectral mixture analysis from a uni-temporal perspective. Int. J. Remote Sens. 27, 645–662.
Quintano, C., Fernández-Manso, A., Shimabukuro, Y.E., Pereira, G., 2012. Spectral unmixing. Int. J. Remote Sens. 33, 5307–5340.
Quintano, C., Fernández-Manso, A., Roberts, D.A., 2013. Multiple endmember spectral mixture analysis (MESMA) to map burn severity levels from Landsat images in Mediterranean countries. Remote Sens. Environ. 136, 76–88.
Quintano, C., Fernández-Manso, A., Calvo, L., Marcos, E., Valbuena, L., 2015. Land surface temperature as potential indicator of burn severity in forest Mediterranean ecosystems. Int. J. Appl. Earth Obs. Geoinf. 36, 1–12.
Quintano, C., Fernández-Manso, A., Roberts, D.A., 2017. Burn severity mapping from Landsat MESMA fraction images and land surface temperatures. Remote Sens. Environ. 190, 83–95.
Quintano, C., Fernandez-Manso, A., Fernandez-Manso, O., 2018. Combination of Landsat and Sentinel-2 MSI data for initial assessing of burn severity. Int. J. Appl. Earth Obs. Geoinf. 64, 221–224.
Quintano, C., Fernández-Manso, A., Calvo, L., Roberts, D.A., 2019. Vegetation and soil fire damage analysis based on species distribution modeling trained with multispectral satellite data. Remote Sens. 11, 1832.
Quintano, C., Fernández-Manso, A., Roberts, D.A., 2020. Enhanced burn severity estimation using fine resolution ET and MESMA fraction images with machine learning algorithm. Remote Sens. Environ. 244, 111815.
Roberts, D.A., Dennison, P.E., Gardner, M., Hetzel, Y., Ustin, S.L., Lee, C., 2003. Evaluation of the potential of hyperion for fire danger assessment by comparison to the airborne visible/infrared imaging spectrometer. IEEE Trans. Geosci. Remote Sens. 41, 1297–1310.
Roberts, D.A., Gardner, M., Church, R., Ustin, S., Scheer, G., Green, R.O., 1998. Mapping chaparral in the Santa Monica Mountains using multiple endmember spectral mixture models. Remote Sens. Environ. 65, 267–279.
Roberts, D.A., Halligan, K., Dennison, P., Dudley, K., Somers, B., Crabbe, A., 2019. Viper Tools User Manual, version 2.1. 92 pp.
Robichaud, P.R., Lewis, S.A., Laes, D.Y.M., Hudak, A.T., Kokaly, R.F., Zamudio, J.A., 2007. Postfire soil burn severity mapping with hyperspectral image unmixing. Remote Sens. Environ. 108, 467–480.
Rodrigues, M., Cunill Camprubí, A., Balaguer-Romano, R., Ruffault, J., Fernandes, P.M., Resco de Rios, V., 2023. Drivers and implications of the extreme 2022 wildfire season in Southwest Europe. Sci. Total Environ. 859, 160320.
Rodriguez-Galiano, V.F., Ghimire, B., Rogan, J., Chica-Olmo, M., Rigol-Sanchez, J.P., 2012. An assessment of the effectiveness of a random forest classifier for land-cover classification. ISPRS J. Photogramm. Remote Sens. 67, 93–104.
Rogan, J., Franklin, J., 2001. Mapping wildfire burn severity in Southern California forests and shrublands using enhanced thematic mapper imagery. Geocarto Int. 16, 91–101.
Roth, K.L., Dennison, P.E., Roberts, D.A., 2012. Comparing endmember selection techniques for accurate mapping of plant species and land cover using imaging spectrometer data. Remote Sens. Environ. 127, 139–152.
Roy, D.P., Boschetti, L., Trigg, S.N., 2006. Remote sensing of fire severity: assessing the performance of the normalized burn ratio. IEEE Geosci. Remote Sens. Lett. 3, 112–116.
Saberi, S.J., Agne, M.C., Harvey, B.J., 2022. Do you CBI what I see? The relationship between the composite burn index and quantitative field measures of burn severity varies across gradients of forest structure. Int. J. Wildland Fire 31, 112–123.
Schaaf, A.N., Dennison, P.E., Fryer, G.K., Roth, K.L., Roberts, D.A., 2011. Mapping plant functional types at multiple spatial resolutions using imaging spectrometer data. GISci.Remote Sens. 48, 324–344.
Shaik, R.U., Laneve, G., Fusilli, L., 2022. An automatic procedure for forest fire fuel mapping using hyperspectral (PRISMA). Remote Sens. 14, 1264.
Singh, P., Pandey, P.C., Petropoulos, G.P., Pavlides, A., Srivastava, P.K., Koutsias, N., Deng, K.A.K., Bao, Y., 2020. Hyperspectral remote sensing in precision agriculture: present status, challenges, and future trends. In: Pandey, P.C., Srivastava, P.K., Petropoulos, G.P. (Eds.), Hyperspectral Remote Sensing. Elsevier, India, pp. 121–146.

Somers, B., Zortea, M., Plaza, A., Asner, G.P., 2012. Automated extraction of image-based endmember bundles for improved spectral unmixing. IEEE J.Select.Top.Appl.Earth Observ.Remote Sens. 5, 396–408.
Soverel, N.O., Perrakis, D.D.B., Coops, N.C., 2010. Estimating burn severity from landsat dNBR and RdNBR indices across western Canada. Remote Sens. Environ. 114, 1896–1909.
Stambaugh, M.C., Hammer, L.D., Godfrey, R., 2015. Performance of burn-severity metrics and classification in oak woodlands and grasslands. Remote Sens. 7, 10501–10522.
Sunderman, S.O., Weisberg, P.J., 2011. Remote sensing approaches for reconstructing fire perimeters and burn severity mosaics in desert spring ecosystems. Remote Sens. Environ. 115, 2384–2389.
Tanase, M.A., de la Riva, J., Pérez-Cabello, F., 2011. Estimating burn severity at the regional level using optically based indices. Can. J. For. Res. 41, 863–872.
Tane, Z., Roberts, D., Veraverbeke, S., Casas, Á., Ramirez, C., Ustin, S., 2018. Evaluating endmember and band selection techniques for multiple endmember spectral mixture analysis using post-fire imaging spectroscopy. Remote Sens. 10, 389.
Tompkins, S., Mustard, J.F., Pieters, C.M., Forsyth, D.W., 1997. Optimization of endmembers for spectral mixture analysis. Remote Sens. Environ. 59, 472–489.
van Wagtendonk, J.W., Root, R.R., Key, C.H., 2004. Comparison of AVIRIS and landsat ETM+ detection capabilities for burn severity. Remote Sens. Environ. 92, 397–408.
Vega, J.A., Fontúrbel, T., Merino, A., Fernández, C., Ferreiro, A., Jiménez, E., 2013. Testing the ability of visual indicators of soil burn severity to reflect changes in soil chemical and microbial properties in pine forests and shrubland. Plant Soil 369, 73–91.
Veraverbeke, S., Stavros, E.N., Hook, J.J., 2014. Assessing fire severity using imaging spectroscopy data from the Airborne Visible/Infrared Imaging Spectrometer (AVIRIS) and comparison with multispectral capabilities. Remote Sens. Environ. 154, 153–163.
Veraverbeke, S., Dennison, P., Gitas, J., Hulley, G., Kalashnikova, O., Katagis, T., Kuai, L., Meng, R., Roberts, D., Stavros, N., 2018. Hyperspectral remote sensing of fire: state-of-the-art and future perspectives. Remote Sens. Environ. 216, 105–121.
Wang, J., Lopez-Lozano, R., Weiss, M., Buis, S., Li, W., Liu, S., Baret, F., Zhang, J., 2022. Crop specific inversion of PROSAIL to retrieve green area index (GAI) from several decametric satellites using a bayesian framework. Remote Sens. Environ. 278, 113085.
Yebra, M., Chuvieco, E., Riaño, D., 2008. Estimation of live fuel moisture content from MODIS images for fire risk assessment. Agric. For. Meteorol. 148, 523–536.
Yin, C., He, B., Yebra, M., Quan, X., Edwards, A.C., Liu, X., Liao, Z., 2020. Improving burn severity retrieval by integrating tree canopy cover into radiative transfer model simulation. Remote Sens. Environ. 236, 111454.
Zambrano-Bigiarini, M., 2020. hydroGOF: Goodness-of-fit functions for comparison of simulated and observed hydrological time seriesR package version 0.4-0. https://doi.org/10.5281/zenodo.839854. https://github.com/hzambran/hydroGOF.
R Core Team (2021). R: A language and environment for statistical computing. R Foundation for Statistical Computing, Vienna, Austria. URL https://www.R-project.org/.